Facile and Rapid Synthesis of Highly Porous Wirelike TiO₂ as Anodes for Lithium-Ion Batteries

H. E. Wang,*[†,‡] Z. G. Lu,[§] L. J. Xi,[†] R. G. Ma,[†] C. D. Wang,[†,‡] J. A. Zapien,*[†,‡] and I. Bello[†,‡]

[†]Department of Physics and Materials Science, City University of Hong Kong, Hong Kong SAR, P.R. China
[‡]Center of Super-Diamond and Advanced Films (COSDAF), City University of Hong Kong, Hong Kong SAR, P.R. China
[§]School of Chemistry and Chemical Engineering, Central South University, Changsha, P.R. China

ABSTRACT: Highly porous wirelike TiO₂ nanostructures have been synthesized by a simple two-step process. The morphological and structural characterizations reveal that the TiO₂ wires typically have diameters from 0.4 to 2 μm, and lengths from 2 to 20 μm. The TiO₂ wires are highly porous and comprise of interconnected nanocrystals with diameters of 8 ± 2 nm resulting in a high specific surface area of 252 m² g⁻¹. The effects of experimental parameters on the structure and morphology of the porous wirelike TiO₂ have been investigated and the possible formation processes of these porous nanostructures are discussed. Galvanostatic charge/discharge tests indicate that the porous wirelike TiO₂ samples exhibit stable reversible lithium ion storage capacities of 167.1 ± 0.7, 152.1 ± 0.8, 139.7 ± 0.3, and 116.1 ± 1.1 mA h g⁻¹ at 0.5, 1, 2, and 5 C rates, respectively. Such improved performance could be ascribed to their unique porous and 1D nanostructures facilitating better electrolyte penetration, higher diffusion rate of electrons and lithium ion, and variation of accommodated volumes during the charge/discharge cycles.

KEYWORDS: anatase, porous wires, hydrothermal synthesis, titanium dioxide, anode, lithium ion battery
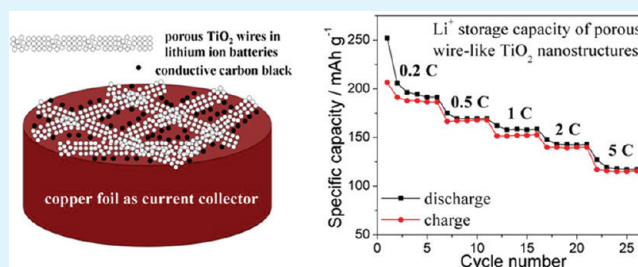
1. INTRODUCTION

Titanium dioxide (TiO₂) is an important semiconductor material with extensive applications in photocatalysis,[1] gas sensing,[2] dye- and quantum dot- sensitized solar cells.[3,4] TiO₂ is also considered as a promising anode material for lithium ion batteries (LIBs) due to its low-cost, excellent chemical stability, relatively high lithium ion (Li⁺) storage capacity, good rate performance, and operation safety.[5] The electrochemical properties of TiO₂ materials strongly depend upon their structural parameters, such as polymorphs, crystallinity, particle size and morphology, specific surface area, and pore structures.[6−11]

In recent years, nanostructured TiO₂ materials, such as nanocrystals (NCs),[9,12−17] one-dimensional (1D) nanostructures[6,8,18−21] and nanoporous microstructures,[11,22−34] have intensively been investigated as anode materials for LIBs to improve the electrode kinetics and storage ability of LIBs. In particular TiO₂ NCs have been studied deeper because their high specific surface area and exposed surfaces can improve electrode reaction kinetics and enhance Li⁺ storage capability at particle surfaces and grain boundaries. However, TiO₂ nanocrystals also have several drawbacks: (i) their preparation and harvesting on a large scale is not convenient; (ii) TiO₂ NCs usually have low packing densities because of their high surface energies and easy aggregation, which lower the LIBs' volumetric energy densities; (iii) the electrodes made of TiO₂ NCs can lose their electronic contact with the current collector after several tens of electrochemical cycling caused by possible

electrochemical aggregation, which leads to degradation and/or loss of electrochemical activities.

Apart from TiO₂ NCs, porous microstructures with interconnected channels have also been intensively investigated as anode materials in LIBs because of their available high internal surface, reduced electron and Li⁺ diffusion length and better packing density.

Various 1D nanostructures, such as nanowires, nanorods, nanotubes, and their arrays, can have better charge transport property because of their specific geometrical characteristics. However, such nanostructures have small surface area compared to NCs and porous microstructures especially when they either have large radial sizes and small aspect ratios or form dense arrays.[35] Such problems may be improved if porous 1D nanostructures can be developed.

Although there are several reports on the fabrication of nanoporous TiO₂ submicro- and microspheres,[36−38] few examples have been demonstrated to synthesize porous 1D TiO₂ nanostructures.[39] Recently, Kim et al.[39] first prepared hydrogen titanate nanowires (H₂Ti₃O₇·nH₂O) by hydrothermal treatment of commercial anatase powders in concentrated NaOH solution followed by ion-exchanging with diluted HCl solution, and then converted them into porous TiO₂ nanowires by subsequent annealing or hydro-

thermal treatment. However, this process involves multiple reaction steps and takes a long reaction period (>3 days). In this work, we report the large-scale synthesis of highly porous, specific surface area of 252 m^2 g^{-1}, wirelike TiO$_2$ nanostructures by a facile and rapid two-step method and their application as anodes for lithium ion batteries.

2. EXPERIMENTAL SECTION

All chemicals were analytical pure grade and used as received. The synthesis of porous wirelike TiO$_2$ structures contains two steps: (i) synthesis of titanium glycolate precursor wires by a microwave-assisted solvothermal process; (ii) transformation of titanium glycolate wires into highly porous anatase TiO$_2$ wires by a microwave-assisted hydrothermal treatment.

2.1. Synthesis of Titanium Glycolate Precursors. In a typical synthetic procedure, 0.5 mL of tetrabutyl titanate (TBT) was dissolved into 20 mL of ethylene glycol (EG) under stirring. The resulting transparent sol was loaded into 35 mL reaction vessel and maintained at 170 °C for 20 min by microwave heating (Discover S-Class, CEM Corporation) along with vigorous stirring. The set pressure limit and heating power were 150 psi and 150 W, respectively. After microwave-assisted solvothermal reaction, the resultant white titanium glycolates precipitates were harvested by centrifugation, followed by rinsing with ethanol several times, and finally drying at 60 °C in air for 12 h.

For comparison, the titanium glycolates were also synthesized by a conventional refluxing process and solvothermal process, respectively. In the refluxing process, 40 mL of EG solution containing 1 mL of TBT was heated in a round-bottom flask under refluxing conditions at 170 °C for 2.5 h along with strong mechanical stirring. In the conventional solvothermal process, 20 mL of EG solution containing 0.5 mL of TBT was transferred into a 25 mL autoclave with a Teflon linear, sealed, and heated in an electric oven at 180 °C for 10 h without any shaking. The synthesized titanium glycolates by these two processes were also harvested by centrifugation, followed by rinsing with ethanol for several times, and finally drying at 60 °C in air for 12 h.

2.2. Synthesis of Porous Wirelike TiO$_2$ Structures. The titanium glycolates precursors were dispersed into 20 mL distilled water and loaded into a 35 mL reaction vial and subjected to microwave-assisted heating at 180 °C for 30 min with set pressure limit and heating power of 180 psi and 150 W, respectively. The final obtained wirelike TiO$_2$ samples were harvested by centrifugation, followed by washing with ethanol, and finally drying at 60 °C in air for 12 h.

2.3. Characterization of the Samples. The crystal structure of the TiO$_2$ samples was analyzed by powder X-ray diffraction (XRD) recorded on a Siemens D500 diffractometer with Cu Kα radiation at room temperature. Surface morphologies of the samples were studied with a Philips XL30 scanning electron microscope (SEM) equipped with a field emission gun (FEG). Transmission electron microscopy (TEM), selected-area electron diffraction (SAED) and high-resolution transmission electron microscopy (HRTEM) analyses were performed with a Philips CM20 transmission electron microscope and a Philips CM200 FEG TEM, respectively. Specific surface area and average pore size distribution were determined by nitrogen adsorption−desorption isotherms at 77 K using a NOVA 1200e Surface Area & Pore Size Analyzer (Quantachrome Instruments). Prior to adsorption experiments, the samples were degassed at 150 °C for 2 h.

The working electrodes for lithium-half cells were prepared by blending a powder mixture consisting of TiO$_2$, carbon black and polyvinylidene difluoride (PVDF) with a weight ratio of 8:1:1 in acetone. The blended slurry was cast onto a copper foil current collector and dried at 120 °C for 10 h in a vacuum oven. CR2025 coin-type cells were assembled with lithium foil as counter electrode and reference electrode, and 1 M LiPF$_6$ dissolved in ethylene carbonate (EC) and dimethyl carbonate (DMC) (1:1 in volume) as electrolyte. Galvanostatic charge−discharge tests were carried out at room temperature with an Arbin Instruments (BT2000, College Station, Texas, USA) system at a voltage region between 1 and 3 V (vs Li$^+$/Li)

at different current rates from 0.2 to 5 C (1 C rate corresponds to the current density of 167.5 mA g^{-1}). Cyclic voltammetry (CV) measurements were recorded on a CHI 660D electrochemical workstation (CH Instruments, Inc.) between 1 and 3 V (vs Li$^+$/Li) at different scan rates from 0.1 to 5 mV s^{-1}.

For comparison, commercial Degussa P25 TiO$_2$ nanoparticles were also used to fabricate lithium-half cells using the same cell-fabrication parameters as described above and tested by galvanostatic charge−discharge experiments.

3. RESULTS AND DISCUSSION

The XRD pattern shown in Figure 1 reveals that all the peaks can be indexed to the pure anatase phase according to JCPDS
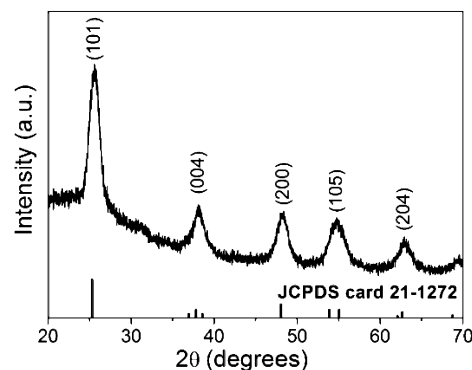

Figure 1. XRD pattern of the as-synthesized porous TiO$_2$ wires.

Card No. 21−1272. The broadening of the diffraction peaks implies the nanocrystalline structure of the TiO$_2$ products or a wide size distribution of the as-synthesized TiO$_2$ samples; the average crystallite size has been estimated according to the Scherrer equation

$$d = k\lambda/\beta\cos\theta \tag{1}$$

where k is a constant (0.89); λ is the X-ray wavelength (0.1541 nm for Cu Kα); β is the full-width at half-maximum for the peak at 2θ = 25.6°; d is the average crystallite size; and θ is the angle of the diffraction peak. The calculated average crystallite size is 6.8 nm based on the (101) peak.

Figure 2 presents the SEM images of the synthesized TiO$_2$ samples. Figure 2a indicates that the TiO$_2$ samples consist of a large quantity of wires with diameters of 0.4 to 2 μm and length of 2−20 μm. The large diameters of some wires are mainly caused by the merging of adjacent wires, while the short wires are due to fractures during the hydrothermal crystallization treatment. A high-magnification SEM image, in Figure 2b, reveals that the TiO$_2$ wires have very coarse surfaces and it appears they are formed from ultrafine nanocrystals with diameters of less than 10 nm.

The microstructure of the prepared TiO$_2$ sample has been further observed by TEM and HRTEM microscopes as depicted in Figure 3. The TEM micrograph of a single TiO$_2$ wire clearly shows that it is highly porous and composed of nanocrystals interconnected with each other. The concentric circles composed of bright spots in the SAED pattern (left inset in Figure 3) demonstrate its polycrystalline nature. The HRTEM micrograph (right inset in Figure 3) further displays the TiO$_2$ wires are composed of spherical nanocrystals with diameter of 8 ± 2 nm and that the mesopores are formed by the assembling of adjacent nanocrystals. Furthermore, the clear

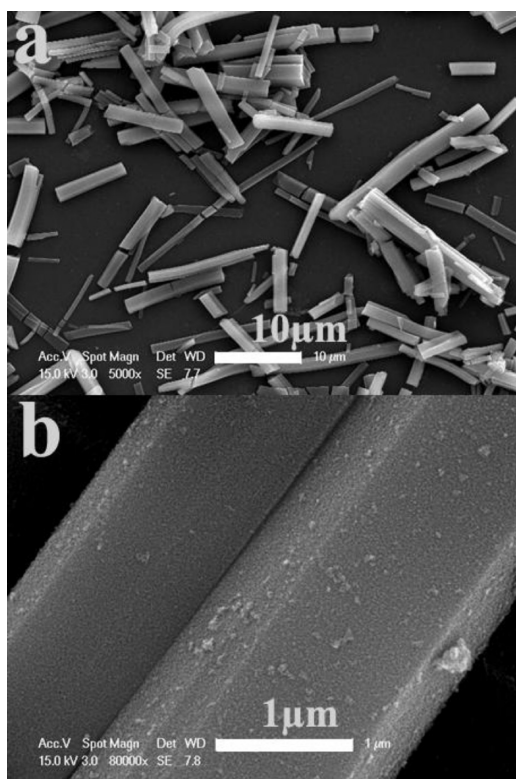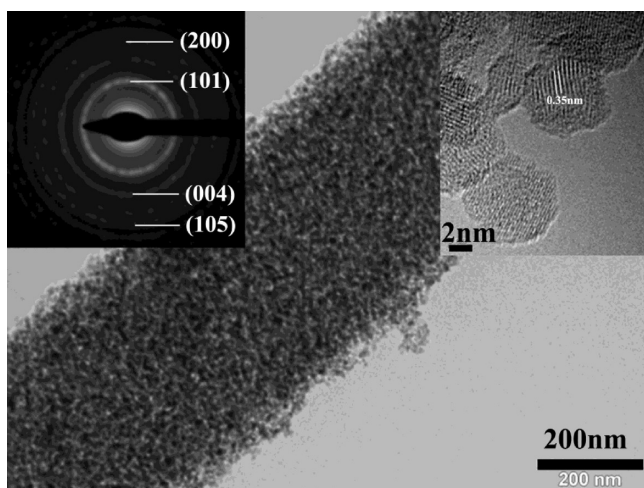**Figure 2.** SEM images of the as-prepared TiO$_2$ samples.

Figure 3. TEM micrograph, SAED pattern (left inset), and HRTEM (right inset) of the prepared TiO$_2$ samples.

lattice fringe with 0.35 nm spacing can be indexed to the (101) crystal plane of anatase TiO$_2$.[30,36,37]

The porous structures of the fabricated TiO$_2$ wires are further investigated by nitrogen adsorption−desorption tests and the Brunauer−Emmett−Teller (BET) adsorption isotherms (Figure 4). As expected, the highly porous characteristics of TiO$_2$ wires in Figure 3 may result in large specific surface area. It is found that the isotherms show a typical type IV curve with a hysteresis loop in the range of 0.5−0.9 P/P_0, which is indicative of a mesoporous feature of the synthesized TiO$_2$ samples.[23,25,26,28,34] The BET specific surface area and pore volume are determined to be 252 m^2 g^{-1} and 0.4 cm^3 g^{-1}, respectively. The pore size distribution calculated from the desorption isotherm using the Barrett−Joyner−Halenda (BJH)
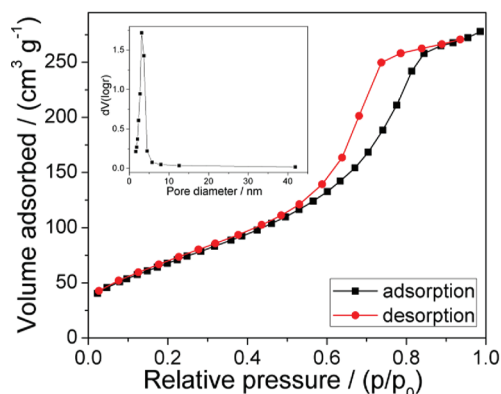

Figure 4. Nitrogen adsorption−desorption isotherms of the porous TiO$_2$ wires and pore size distribution calculated from the desorption isotherm using the Barrett−Joyner−Halenda (BJH) analysis method (inset).

method (inset image in Figure 4) indicates the presence of rather uniform mesopores with an average pore diameter of 3.1 nm in the TiO$_2$ wires.

In the following part, we investigate the effects of experimental parameters on the fabrication of the porous wirelike TiO$_2$. We notice that the concentration of TBT in EG and the stirring play a key role in the formation of wirelike titanium glycolate precursors. First, no titanium glycolate precipitates are produced when either the dosage of TBT is less than 0.05 mL or the microwave-assisted solvothermal reaction is performed without vigorous stirring. In addition, it is found that: (i) the direct annealing of the titanium glycolate precursors only results in compact wirelike TiO$_2$ samples without any pores (Figure 5a), which is consistent with the previous reports on dense TiO$_2$ spheres[40−42] and wires;[43] (ii) large quantities of bulk particles are obtained by the conventional refluxing process carried out at 170 °C for 2.5 h along with mechanical stirring (Figure 5b); (iii) only very few discrete particles could be obtained by the conventional solvothermal reaction performed at 180 °C for 10 h without
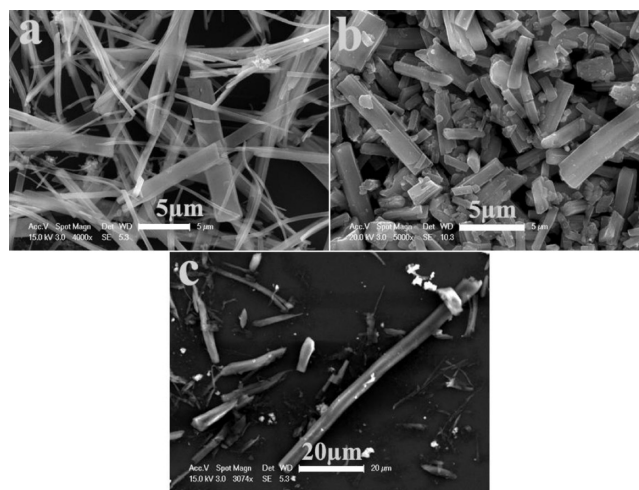

Figure 5. SEM images of the samples synthesized under different conditions: (a) TiO$_2$ wires obtained by annealing the titanium glycolate precursors at 500 °C for 2 h; (b) titanium glycolate precursors obtained by refluxing the reaction sols at 170 °C for 2.5 h; (c) titanium glycolates synthesized by hydrothermal treatment of the reaction sol at 180 °C for 10 h.
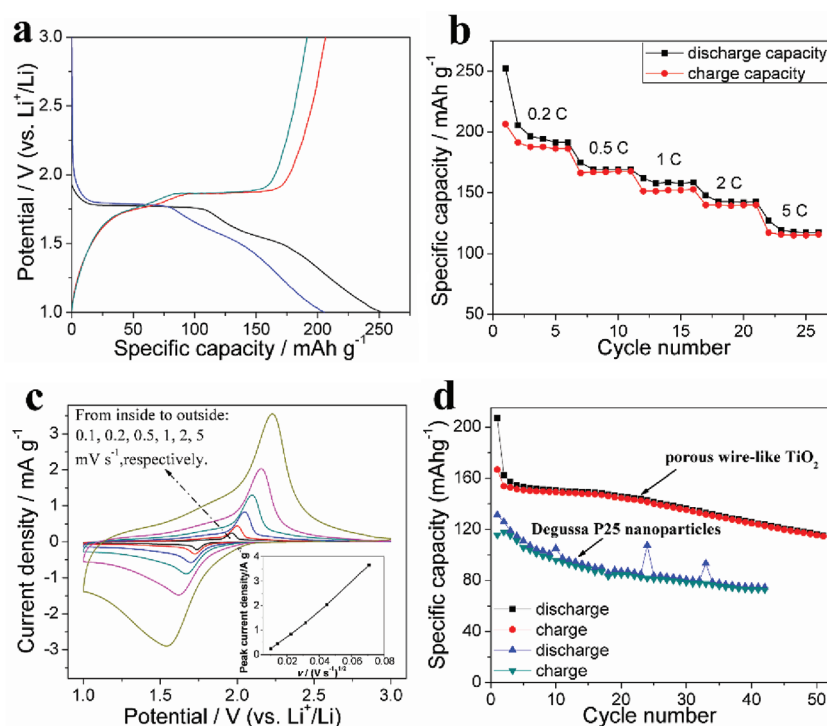
Figure 6. (a) First and second discharge−charge curves of the porous wirelike TiO_2 electrodes at 0.2 C rate; (b) specific capacities of the TiO_2 electrodes tested at different rates; (c) cyclic voltammetry profiles of the TiO_2 electrodes measured at different scan rates; (d) cycle performances of the porous wirelike TiO_2 electrodes and commercial Degussa P25 nanoparticles activated at 0.2 C for 1 cycle and then cycled at 0.625 C between a potential window of 1.3−2.5 V.

shaking (Figure 5c). Therefore, the current microwave-assisted solvothermal route provides a quick and large-scale strategy for the synthesis of highly porous TiO_2 wires.

It is known that TBT is very reactive with water and white precipitates can be produced quickly even from contact with moisture. However, its reactivity can be lowered by alkoxy chain-exchange reaction with EG as expressed in eq 2[40]

$$Ti(OC_4H_9)_4 + 2HO(C_2H_4)OH$$
$$\rightarrow Ti((OCH_2)_2)_2 + 4C_4H_9OH \quad (2)$$
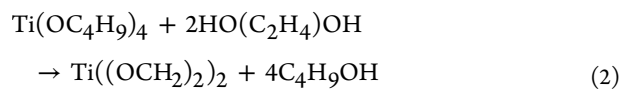
The resulting chainlike coordination titanium glycolate complexes in eq 2 are more resistant to hydrolysis. When the EG solution containing titanium glycolate is microwave heated at 170 °C for 20 min along with vigorous stirring, the chainlike complexes will become long and tend to aggregate into bundles, which results in the formation of wirelike titanium glycolate precipitates from the reaction solution.[43]

Next, porous anatase TiO_2 wires can further be synthesized by a subsequent microwave-assisted hydrothermal treatment of the titanium glycolate precursors. In this hydrothermal process, the amorphous titanium glycolates have a loose structure and can promptly react with water to lose their alkoxy groups and form initial TiO_2 nuclei subjected to the microwave heating. The reaction equation can be formulated as follows

$$Ti((OCH_2)_2)_2 + 2H_2O \rightarrow TiO_2 + 2HO(CH_2)_2OH$$
$$(3)$$
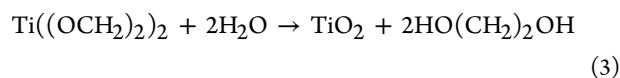
In general, the density difference between titanium glycolates and TiO_2 can result in occasional formation of cracks on the wires' surface, which facilitates the penetration of water and releases the alkoxy groups from inside the wires. This reaction proceeds rapidly and continuously accompanying the growth of

the TiO_2 nuclei under the microwave heating resulting in porous anatase TiO_2 wires comprising interconnected nano-crystals.[38]

The one-dimensional, nanoporous, and high specific surface area features of the pristine wirelike TiO_2 are attractive characteristics in a large range of applications such as catalysis, gas sensing, energy conversion and storage among others. In this work, we evaluate the electrochemical performance of the porous wirelike TiO_2 samples as anodes for lithium ion batteries.

The Li^+ insertion into and extraction from TiO_2 matrix can be formulated by the following reaction equation

$$TiO_2 + xLi^+ + xe^- \rightarrow Li_xTiO_2 \ (0 \leq x \leq 1) \quad (4)$$

The first two discharge−charge curves of the porous wirelike TiO_2 electrodes at 0.2 C are shown in Figure 6a. Both the discharge and charge curves exhibit well-defined voltage profiles which are characteristic of anatase TiO_2. The plateaus of discharge and charge are located at 1.78 ± 0.01 and 1.87 ± 0.01 V, respectively. The discharge curve of the TiO_2 electrodes can be divided into three domains. The first domain is a monotonous potential drop caused by a solid solution insertion mechanism linked to the small nanocrystallite size and porous nanostructures.[9] The second domain with a potential plateau at 1.78 ± 0.01 V corresponds to Li^+ intercalation into the interstitial octahedral site of TiO_2. In this process a two-phase reaction occurs with phase equilibrium of tetragonal Li-poor $Li_{0.01}TiO_2$ and orthorhombic Li-rich $Li_{0.6}TiO_2$.[44,45] The third domain with a slope potential drop relates to the Li^+ storage at the surface as well as the formation of $LiTiO_2$ phase.[12] The initial discharge and charge capacities of the porous wirelike TiO_2 structures are 252.2 and 206.4 mA h g^{-1}, respectively, with an irreversible capacity of 45.8 mA h g^{-1} and a columbic

efficiency of 81.8%. This irreversible capacity loss is mainly caused by insertion of some Li^+ into sites that are not extractable and decomposition of trace water adsorbed on the TiO_2 electrode surfaces.[46] In the second cycle, the discharge and charge capacities are reduced to 205.7 and 191.5 mA h g^{-1}, respectively. However, the columbic efficiency (93.1%) has been significantly improved, suggesting that the Li^+ intercalation and deintercalation are highly reversible. Figure 6b shows the rate capability of the porous wirelike TiO_2 electrodes. It reveals that the discharge and charge capacities of the TiO_2 electrodes decrease along with the increase of current densities. However, the electrodes still have highly stabilized Li^+ storage capacities of 167.1 ± 0.7, 152.1 ± 0.8, 139.7 ± 0.3, and 116.1 ± 1.1 mA h g^{-1} at 0.5, 1, 2, and 5 C rates, which are comparable to those of mesoporous nanospheres (153.6 ± 1.9 mA h g^{-1} at 1 C and 131.7 ± 3.7 mA h g^{-1} at 5 C),[28] nanoporous mesocrystals (164.9 mAh g^{-1} at 1 C and 151.7 mA h g^{-1} at 2 C),[30] mesoporous microspheres (175 mA h g^{-1} at 0.6 C and 156 mA h g^{-1} at 1.2 C),[31] and better than those of dense nanofibers (108.9 ± 1.8 mA h g^{-1} at 0.4 C and 92.8 ± 3.5 mA h g^{-1} at 1 C)[21] or nanoparticles (115.1 ± 1.9 mA h g^{-1} at 1 C and 109.4 ± 3.8 mA h g^{-1} at 2 C).[30]

To further understand the electrochemical reaction processes during the discharge/charge cycles, we recorded cyclic voltammetry (CV) profiles between 1 and 3 V at different scan rates as shown in Figure 6c. A pair of reduction/oxidation peaks located at 1.73 ± 0.01 and 1.96 ± 0.01 V are clearly observed during the cathodic and anodic processes at a scan rate of 0.1 mV s^{-1}, which are characteristic of Li^+ intercalation and deintercalation into/from anatase and consistent with the results shown in the discharge–charge tests in Figure 6a. A 0.23 V interval between the cathodic/anodic peaks, determined by the overpotential required for the transformation between TiO_2 and Li_xTiO_2 phases, is lower than that of the values (0.33−0.43 V) available in the literatures.[21,30,31] The lower peak potential interval reveals that the Li^+ intercalation/deintercalation reactions proceed more easily in the porous wirelike TiO_2 samples. In addition, the ratio of the cathodic and anodic peak current, i_{pc}/i_{pa}, is close to 1, suggesting that Li^+ is reversibly intercalated and deintercalated, and this redox system remains in equilibrium throughout the whole potential scan. These results demonstrate a very good reaction kinetics for Li^+ insertion in the porous wirelike TiO_2 electrodes. The inset image in Figure 6c shows that the anodic peak current has a linear relationship with the square root of the scan rate, suggesting a Li^+ diffusion limited electrochemical process.[21,29]

Figure 6d shows the cycling performances of porous wirelike TiO_2 and commercial Degussa P25 nanoparticles activated at 0.2 C for 1 cycle and then cycled at 0.625 C between a potential region of 1.3−2.5 V. The results reveal that the lithium-half cells assembled with porous TiO_2 wires exhibit high initial Li^+ storage capacity (166.6 mA h g^{-1}) and stable cycling performance during the first 20 cycles (144.5 mA h g^{-1} over 20 cycles). Next, the cell displays a gradual capacity fading along with cycling. The charge capacity of porous TiO_2 wires over 51 cycles is 114.4 mA h g^{-1}, with a capacity retention rate of 68.7%. In contrast, the commercial Degussa P25 nanoparticles exhibit a low initial Li^+ storage capacity (115.4 mA h g^{-1}), and a continuous capacity fading during the charge–discharge process. The charge capacity of P25 nanoparticles over 42 cycles is 72.7 mA h g^{-1}, with a capacity retention rate of 63%, which is much inferior to that of porous TiO_2 wires. The poor cycle performance of commercial P25 nanoparticles has

also been observed by Wohlfahrt-Mehrens et al.,[23] which can be caused by the aggregation of nanoparticles and loss of electric contact with current contact during the charge−discharge process.

The superior electrochemical properties of the prepared porous wirelike TiO_2 electrodes can mainly be ascribed to their distinct porous and 1D structural characteristics, as schematically illustrated in Figure 7: (i) the porous wires can form a 3D
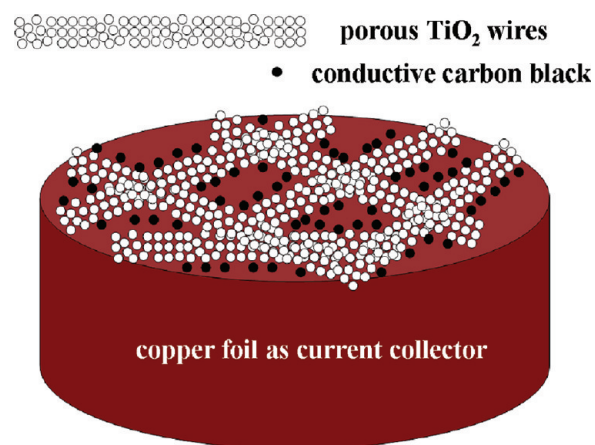

Figure 7. Schematic illustration of the porous wirelike TiO_2 electrodes used in lithium ion batteries.

network with hierarchical pore structures (large voids among the adjacent wires and mesopores on single wire) for better electrolyte penetration and mass transfer; (ii) the interconnected channels shorten the Li^+ and electron diffusion lengths; (iii) the 1D geometry improves the electrons transport along both the radial and axial directions; (iv) the highly porous nanostructures can effectively alleviate the volume variation upon lithiation and delithiation processes.

However, it is noticed that the electrochemical performance of the porous TiO_2 wires should be further improved for practical applications in lithium-ion batteries, which can be implemented by the following aspects. First, the structural parameters of the porous TiO_2 wires (e.g., particle size and size distribution, crystallization, pore size and pore distribution) can be further tailored by optimizing the experimental parameters. Second, the coating of the active materials on the current collector can be improved by optimizing the coating techniques to increase the tap density. Last but not least, surface coating of the TiO_2 samples with a thin layer of carbon can be performed to increase the electronic conductivity of TiO_2 materials.[28]

4. CONCLUSIONS

Porous wirelike TiO_2 nanostructures have been synthesized by a simple two-step process. The TiO_2 samples are highly porous structures with a high specific surface area as large as 252 m^2 g^{-1}. The porous wirelike TiO_2 samples exhibit superior electrochemical performance with a good combination of high specific capacity (206.4 mA h g^{-1} at 0.2 C) and remarkable rate capability (167.1 ± 0.7 and 116.1 ± 1.1 mA h g^{-1} at 0.5 and 5 C, respectively). This improved electrochemical performance of the TiO_2 samples can be attributed to their distinct porous and 1D characteristics. The pristine porous wirelike TiO_2 nanostructures may also have potential applications in dye- and quantum-dot sensitized solar cells because of their high surface area, 1D geometry, and large particle size.

■ AUTHOR INFORMATION

Corresponding Author

*E-mail: hongen.wang@gmail.com (H.E.W.); apjazs@cityu. edu.hk (J.A.Z.).

Notes

The authors declare no competing financial interest.

■ REFERENCES

(1) Fujishima, A.; Hongda, K. *Nature* **1972**, *238*, 37−38.

(2) Benkstein, K. D.; Semancik, S. *Sens. Actuators B* **2006**, *113*, 445−453.

(3) O'Regan, B.; Gratzel, M. *Nature* **1991**, *353*, 737−740.

(4) Kamat, P. V.; Tvrdy, K.; Baker, D. R.; Radich, J. G. *Chem. Rev.* **2010**, *110*, 6664−6688.

(5) Wagemaker, M.; Kentgens, A. P. M; Mulder, F. M. *Nature* **2002**, *418*, 397−399.

(6) Armstrong, A. R.; Armstrong, G.; Canales, J.; Garcia, R.; Bruce, P. G. *Adv. Mater.* **2005**, *17*, 862−865.

(7) Dambournet, D.; Belharouak, I.; Amine, K. *Chem. Mater.* **2010**, *22*, 1173−1179.

(8) Fang, H. T.; Liu, M.; Wang, D. W.; Sun, T.; Guan, D. S.; Li, F.; Zhou, J. G.; Sham, T. K.; Cheng, H. M. *Nanotechnology* **2009**, *20*, 225701.

(9) Sudant, G.; Baudrin, E.; Larcher, D.; Tarascon, J. M. *J. Mater. Chem.* **2005**, *15*, 1263−1269.

(10) Sun, C. H.; Yang, X. H.; Chen, J. S.; Li, Z.; Lou, X. W.; Li, C. Z.; Smith, S. C.; Lu, G. Q.; Yang, H. G. *Chem. Commun.* **2010**, *46*, 6129−6131.

(11) Wang, H. E.; Cheng, H.; Liu, C. P.; Chen, X.; Jiang, Q. L.; Lu, Z. G.; Li, Y. Y.; Chung, C. Y.; Zhang, W. J.; Zapien, J. A.; Martinu, L.; Bello, I. *J. Power Sources* **2011**, *196*, 6394−6399.

(12) Wagemaker, M.; Borghols, W. J. H.; Mulder, F. M. *J. Am. Chem. Soc.* **2007**, *129*, 4323−4327.

(13) Subramanian, V.; Karki, A.; Gnanasekar, K. I.; Eddy, F. P.; Rambabu, B. *J. Power Sources* **2006**, *159*, 186−192.

(14) Kubiak, P.; Pfanzelt, M.; Geserick, J.; Hormann, U.; Husing, N.; Kaiser, U.; Wohlfahrt-Mehrens, M. *J. Power Sources* **2009**, *194*, 1099−1104.

(15) Chen, J. S.; Lou, X. W. *J. Power Sources* **2010**, *195*, 2905−2908.

(16) Sasidharan, M.; Nakashima, K.; Gunawardhana, N.; Yokoi, T.; Inoue, M.; Yusa, S. I.; Yoshio, M.; Tatsumi, T. *Chem. Commun.* **2011**, *47*, 6921−6923.

(17) Lafont, U.; Carta, D.; Mountjoy, G.; Chadwick, A. V.; Kelder, E. M. *J. Phys. Chem. C* **2010**, *114*, 1372−1378.

(18) Liu, D. W.; Xiao, P.; Zhang, Y. H.; Garcia, B. B.; Zhang, Q. F.; Guo, Q.; Champion, R.; Cao, G. Z. *J. Phys. Chem. C* **2008**, *112*, 11175−11180.

(19) Li, Y. M.; Lv, X. J.; Li, J. H. *Appl. Phys. Lett.* **2009**, *95*, 113102.

(20) Kim, S. W.; Han,vT., H.; Kim, J.; Gwon, H.; Moon, H. S.; Kang, S. W.; Kim, S. O.; Kang, K. *ACS Nano* **2009**, *3*, 1085−1090.

(21) Nam, S. H.; Shim, H. S.; Kim, Y. S.; Dar, M. A.; Kim, J. G.; Kim, W. B. *ACS Appl. Mater. Interfaces* **2010**, *2*, 2046−2052.

(22) Guo, Y. G.; Hu, Y. S.; Sigle, W.; Maier, J. *Adv. Mater.* **2007**, *19*, 2087−2091.

(23) Kubiak, P.; Geserick, J.; Husing, N.; Wohlfahrt-Mehrens, M. *J. Power Sources* **2008**, *175*, 510−516.

(24) Wang, D. H.; Choi, D.; Yang, Z. G.; Viswanathan, V. V.; Nie, Z. M.; Wang, C. M.; Song, Y. J.; Zhang, J. G.; Liu, J. *Chem. Mater.* **2008**, *20*, 3435−3442.

(25) Yue, W. B.; Xu, X. X.; Irvine, J. T. S.; Attidekou, P. S.; Liu, C.; He, H. Y.; Zhao, D. Y.; Zhou, W. Z. *Chem. Mater.* **2009**, *21*, 2540−2546.

(26) Jung, H. G.; Yoon, C. S.; Prakash, J.; Sun, Y. K. *J. Phys. Chem. C* **2009**, *113*, 21258−21263.

(27) Chen, J. Z.; Yang, L.; Tang, Y. F. *J. Power Sources* **2010**, *195*, 6893−6896.

(28) Cao, F. F.; Wu, X. L.; Xin, S.; Guo, Y. G.; Wan, L. J. *J. Phys. Chem. C* **2010**, *114*, 10308−10313.

(29) Das, S. K.; Darmakolla, S.; Bhattacharyya, A. J. *J. Mater. Chem.* **2010**, *20*, 1600−1606.

(30) Ye, J. F.; Liu, W.; Cai, J. G.; Chen, S.; Zhao, X. W.; Zhou, H. H.; Qi, L. M. *J. Am. Chem. Soc.* **2011**, *133*, 933−940.

(31) Wang, J.; Zhou, Y. K.; Hu, Y. Y.; O'Hayre, R.; Shao, Z. P. *J. Phys. Chem. C* **2011**, *115*, 2529−2536.

(32) Yoon, S.; Manthiram, A. *J. Phys. Chem. C* **2011**, *115*, 9410−9416.

(33) Chen, J. S.; Tan, Y. L.; Li, C. M.; Cheah, Y. L.; Luan, D. Y.; Madhavi, S.; Boey, F. Y. C.; Archer, L. A.; Lou, X. W. *J. Am. Chem. Soc.* **2010**, *132*, 6124−6130.

(34) Liu, H. S.; Bi, Z. H.; Sun, X. G.; Unocic, R. R.; Paranthaman, M. P.; Dai, S.; Brown, G. M. *Adv. Mater.* **2011**, *23*, 3450−3454.

(35) Wang, H. E.; Chen, Z. H.; Leung, Y. H.; Luan, C. Y.; Liu, C. P.; Tang, Y. B.; Yan, C.; Zhang, W. J.; Zapien, J. A.; Bello, I; Lee, S. T. *Appl. Phys. Lett.* **2010**, *96*, 263104.

(36) Zhong, L. S.; Hu, J. S.; Wan, L. J.; Song, W. G. *Chem. Commun.* **2008**, 1184−1186.

(37) Chen, D. H.; Cao, L.; Huang, F. Z.; Imperia, P.; Cheng, Y. B.; Caruso, R. A. *J. Am. Chem. Soc.* **2010**, *132*, 4438−4444.

(38) Wang, H. E.; Zheng, L. X.; Liu, C. P.; Liu, Y. K.; Luan, C. Y.; Cheng, H.; Li, Y. Y.; Martinu, L.; Zapien, J. A.; Bello, I. *J. Phys. Chem. C* **2011**, *115*, 10419−10425.

(39) Shim, H. W.; Lee, D. K.; Cho, I. S.; Hong, K. S.; Kim, D. W. *Nanotechnology* **2010**, *21*, 255706.

(40) Jiang, X. C.; Herricks, T.; Xia, Y. N. *Adv. Mater.* **2003**, *15*, 1205−1209.

(41) Pal, M.; Serrano, J. G.; Santiago, P.; Pal, U. *J. Phys. Chem. C* **2007**, *111*, 96−102.

(42) Wang, H.; Li, B.; Yan, Z. X.; Lu, Z. G.; Cheng, R. J.; Qian, D. *Rare Met.* **2008**, *27*, 1−4.

(43) Jiang, X. C.; Wang, Y. L.; Herricks, T.; Xia, Y. N. *J. Mater. Chem.* **2004**, *14*, 695−703.

(44) Cava, R. J.; Murphy, D. W.; Zahurak, S. *J. Solid State Chem.* **1984**, *53*, 64−75.

(45) Wagemaker, M.; Kearley, G. J.; Well, A. A. W.; Mutka, H.; Mulder, F. M. *J. Am. Chem. Soc.* **2003**, *125*, 840−848.

(46) Borghols, W. J. H.; Lutzenkirchen-Hecht, D.; Haake, U.; Chan, W.; Lafont, U.; Kelder, E. M.; Eck, E. R. H.; Kentgens, A. P. M; Mulder, F. M.; Wagemaker, M. *J. Electrochem. Soc.* **2010**, *157*, A582−A588.